



# Modeling thermal and irradiation-induced swelling effects on the integrity of $\text{Ti}_3\text{SiC}_2/\text{SiC}$ joints



Ba Nghiep Nguyen<sup>\*</sup>, Charles H. Henager Jr., Richard J. Kurtz

Pacific Northwest National Laboratory, P.O. Box 999, Richland, WA 99352, United States

## ARTICLE INFO

### Article history:

Received 7 March 2017

Received in revised form

10 August 2017

Accepted 6 September 2017

Available online 8 September 2017

### Keywords:

SiC

Fusion materials

Joining

Swelling

Neutron irradiation

Thermal expansion

Damage modeling

Finite element

## ABSTRACT

Previously, results for CVD-SiC joined by a solid state displacement reaction to form a dual-phase SiC/MAX phase joint subsequently irradiated at 800 °C to 5 dpa indicated some cracking in the joint. This paper elucidates the cracking origin by developing a model that accounts for differential thermal expansion and irradiation-induced swelling between the substrate and joint materials by using a continuum damage mechanics approach with support from micromechanical modeling. Damage accumulation in joined specimens irradiated at four temperatures (300 °C, 400 °C, 500 °C and 800 °C) is analyzed. We assume the experimental irradiation dose is sufficient to cause saturation swelling in SiC. The analyses indicate that the SiC/MAX joint survives irradiation-induced swelling at all the irradiation temperatures considered. The joint experiences only minor damage when heated to and irradiated at 800 °C as well as cooling to room temperature. The prediction agrees with the experimental findings available for this case. However, the joint heated to 300 °C suffers severe damage during irradiation-induced swelling at this temperature, and additional damage after cooling to room temperature. Irradiation at 400 °C and subsequent cooling to room temperature produced similar damage to the irradiation 300 °C case, but to a lesser extent. The joint heated to 500 °C and irradiated at this temperature suffered only very minor damage, but further moderate damage occurred after cooling to room temperature.

© 2017 Elsevier B.V. All rights reserved.

## 1. Introduction

There has been a demonstrable and critical need to develop methods for joining silicon carbide (SiC) to itself or other materials to enable application of SiC ceramics and composites in future fusion reactors or nuclear systems since it is difficult to fabricate an entire composite structure without some joined sections. The international fusion materials community has recently irradiated and tested several joint types and compositions including  $\text{Ti}_3\text{SiC}_2/\text{SiC}$  composite joints in the High Flux Isotope Reactor (HFIR) reactor at Oak Ridge National Laboratory (ORNL) [1]. As discussed in Ref. [1], joining SiC to itself or to other materials is a critical technological need that has not been resolved and two key issues central to this technology are identified in Ref. [1]. The first issue is the rather poor irradiation stability that was observed from the limited data

available on the irradiation of several joints, which included the joined SiC material. The second issue is the lack of a widely accepted standard test method for joining that can be successfully irradiated and tested to provide high-quality strength data.

In addition, there is a general lack of predictive modeling tools that can either assist in designing a ceramic joint to withstand irradiation, or provide guidance to develop a joining method for SiC and its composites. As discussed in Ref. [1] it was not possible to predict in advance which of the joints would either be successful or would even survive the irradiation. This paper attempts to address the lack of modeling tools by developing a damage model to elucidate the origin of cracking observed in ceramic joints subjected to heating followed by neutron irradiation at elevated temperatures (up to 800 °C). The model relies on continuum damage mechanics (CDM) in its formulation and uses micromechanical modeling to identify the material parameters or properties that are not known or available.

The modeling work in this paper is performed for the MAX-phase joining method in which a composite made of SiC and  $\text{Ti}_3\text{SiC}_2$  is produced using the displacement reaction between SiC

<sup>\*</sup> Corresponding author. Pacific Northwest National Laboratory, PO Box 999, MSIN: J4-55, Richland, WA 99352, United States.

E-mail address: [Ba.Nguyen@pnnl.gov](mailto:Ba.Nguyen@pnnl.gov) (B.N. Nguyen).

and TiC [2]:  $3\text{TiC} + 2\text{Si} \rightarrow \text{Ti}_3\text{SiC}_2 + \text{SiC}$  (3C-SiC polytype). Pacific Northwest National Laboratory (PNNL) has developed a tape casting process to join ceramics using this reaction [3]. Our previous modeling work using CDM for the unirradiated  $\text{Ti}_3\text{SiC}_2/\text{SiC}$  joint and a SiC joint subjected to torsion was reported in Ref. [4]. The  $\text{Ti}_3\text{SiC}_2$  MAX phase joining for SiC was subsequently evaluated for the effects of irradiation at 800 °C [1], however, the effects of neutron irradiation on integrity are limited or largely unknown for both bulk materials and joined structures at other irradiation temperatures. Fortunately, there is now enough basic data for the constituents of this joint so that an improved model can be developed that can help understand joint behavior following thermomechanical and irradiation exposures. It is hoped that this modeling method can be used to help design improved joints for future irradiation tests by indicating material incompatibilities in advance of expensive in-reactor exposure tests.

## 2. Problem formulation

### 2.1. Statement of the problem

A typical miniature torsion hourglass (THG) specimen with a fully bonded joint is shown in Fig. 1 [1,4] that was used in the HFIR irradiation study tested at 800 °C and 5 dpa. This paper studies the same THG specimen made of CVD-SiC substrates joined by a 15- $\mu\text{m}$   $\text{Ti}_3\text{SiC}_2/\text{SiC}$  dual-phase bonding layer or joint. Before testing, SEM examinations indicated no transverse cracks or microcracks in the joint or at the joint/SiC interfaces. After the irradiation experiment, microcracks were found within the  $\text{Ti}_3\text{SiC}_2/\text{SiC}$  joint material, but no extensive propagation within the joint was observed. No irradiation experiments were reported at temperatures lower than 800 °C for the  $\text{Ti}_3\text{SiC}_2/\text{SiC}$ -joined CVD-SiC specimens with the joints processed by the tape casting method using displacement reactions between SiC and TiC although Ref. [1] reports experiments at 500 °C and 3 dpa for similar THG specimens containing different bonding layers. More recently, Koyanagi et al. [5] reported the neutron irradiation effects on  $\text{Ti}_3\text{SiC}_2/\text{SiC}$ -joined CVD SiC at  $\sim 300$  °C. In Ref. [5], the 150- $\mu\text{m}$  joint was formed from the reaction sintering with a Ti-Si-C system according to proprietary process methods.

The objective of this research is to understand through numerical analyses the origin of microcracking in THG specimens

containing a  $\text{Ti}_3\text{SiC}_2/\text{SiC}$  joint and to predict damage initiation and development in these specimens subjected to heating to selected temperatures and neutron irradiation at those temperatures. Four irradiation temperatures are considered: 300 °C, 400 °C, 500 °C and 800 °C. A continuum damage modeling approach with support from micromechanical modeling is developed. In this paper, irradiation directly causing material degradation that affects mechanical properties is not modeled, but the modeling approach accounts for the *irradiation-induced swelling* that can cause subsequent damage, particularly if the material is constrained to deformation. We first compare our damage predictions with the available experimental observations reported in Ref. [1] for the irradiation test at 800 °C. We then apply the damage model to predict damage development for the tests at 300 °C, 400 °C, and 500 °C.

### 2.2. Constitutive modeling

The continuum damage mechanics (CDM) model formulated here to account for the material thermal expansion combined with the irradiation-induced swelling is derived from a model by Nguyen et al. [6] that was reformulated in Ref. [4] for unirradiated THG specimens subjected to torsion. The constitutive relations of the elastic damage model derived from a thermodynamic potential

$$\Phi(\epsilon_{ij}^m, T, D) = \frac{1}{2} C_{ijkl}(T, D) \epsilon_{ij}^m \epsilon_{kl}^m \quad (1)$$

is written as:

$$\begin{aligned} \sigma_{ij} &= C_{ijkl}(T, D) (\epsilon_{kl} - \epsilon_{kl}^{\text{th}} - \epsilon_{kl}^s) = C_{ijkl}^0(T) (1 - D) (\epsilon_{kl} - \epsilon_{kl}^{\text{th}} - \epsilon_{kl}^s) \\ &= C_{ijkl}^0(T) (1 - D) \epsilon_{kl}^m \end{aligned} \quad (2)$$

where  $C_{ijkl}(T, D)$  is the material elastic stiffness tensor that varies with temperature  $T$  and is affected by the microcracking damage phenomenologically described by the damage variable,  $D$ . A linear stiffness reduction law of  $C_{ijkl}(T, D)$  with  $D$  is used in Eq. (2) for isotropic damage where  $C_{ijkl}^0(T)$  is the initial stiffness tensor without material damage.  $\epsilon_{ij}$ ,  $\epsilon_{ij}^{\text{th}}$ ,  $\epsilon_{ij}^m$  and  $\epsilon_{ij}^s$  are the total, thermal, mechanical, and swelling strains, respectively. In Eq. (1), decoupling between the damage, thermal and swelling effects is assumed, and for a given temperature, the elastic stiffness tensor is assumed to vary linearly with  $D$ . In addition, the current phenomenological model describes damage due to *thermomechanical* loadings. At this stage of the development, the model can account for the degraded stiffness due to irradiation in a simple manner by replacing the virgin stiffness tensor  $C_{ijkl}^0(T)$  in Eq. (2) by the irradiation-reduced stiffness  $C_{ijkl}^{0,*}(T, S)$  due to irradiation at a given dose and temperature based on measured data.  $C_{ijkl}^{0,*}(T, S)$  is also a function of the irradiation-induced swelling magnitude,  $S$ . Irradiation generally reduces the elastic modulus with greater reduction for lower irradiation temperatures as discussed in Ref. [7]. For the irradiation temperatures considered in this work, the modulus reduction is rather small for CVD SiC ( $\sim 5\%$ ). While modulus reduction data as a function of dose and temperature are available for SiC [7], such data do not exist for the MAX phase  $\text{Ti}_3\text{SiC}_2/\text{SiC}$  composite. In this work, we neglect the damage directly caused by neutron irradiation for the CVD-SiC and MAX phase composite studied. Thus, damage in the material is induced only by the mechanical deformation resulting from thermal expansion and irradiation-induced swelling.

The thermal strain tensor  $\epsilon_{ij}^{\text{th}}$  is computed in terms of the

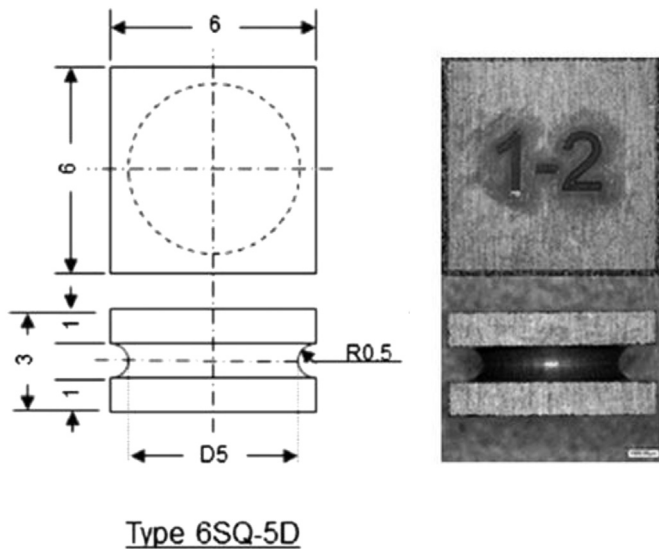


**Fig. 1.** The miniature torsion specimen tested and studied in Refs. [1,4] and used in this study, (a) a schematic geometrical description with dimensions in mm, and (b) an optical image.

temperature-dependent coefficients of thermal expansion (CTEs)  $\alpha_{ij}(T)$  and temperature change  $\Delta T$  as:

$$\epsilon_{ij}^{\text{th}} = \alpha_{ij}(T) \Delta T \quad (3)$$

For incorporation of the irradiation-induced swelling strain tensor  $\epsilon_{ij}^s$ , we use a model proposed by Ben-Belgacem et al. [8] which is expressed in terms of the swelling strains as:

$$\epsilon_{ij}^s = \begin{cases} S_{ij}(T) & \text{if } i = j \text{ and } i, j = 1, \dots, 3 \\ 0 & \text{if } i \neq j \end{cases} \quad (4)$$

where  $S_{ij}(T)$  denotes the non-zero swelling strain components. If isotropic swelling is assumed, Equation (4) becomes:

$$\epsilon_{ij}^s = \frac{S(T)}{3} \delta_{ij} \quad (5)$$

with  $\delta_{ij} = \begin{cases} 1 & \text{if } i = j \text{ and } i, j = 1, \dots, 3 \\ 0 & \text{if } i \neq j \end{cases}$  and where  $S$  denotes the swelling strain magnitude. In this work  $S$  can increase from 0 to a maximum prescribed value,  $S_{\text{max}}$ , that is in general a function of the irradiation temperature and swelling regime.  $S$  represents the volumetric strain caused by irradiation-induced swelling. In this work, we consider isotropic swelling and the experimental irradiation doses in a range leading to saturation swelling in SiC. Thus  $S_{\text{max}}$  for SiC at a given irradiation temperature corresponds to the saturation swelling value at that temperature. The thermal and swelling strains are treated similarly in the continuum mechanics framework here; however, Eqs. (3) and (4) clearly show that thermal strains vanish if the temperature change is reduced to zero whereas irradiation-induced swelling strains subsist after irradiation.

The damage evolution law was obtained using the concepts of thermodynamics of continuous media [9–11] and a damage criterion dependent on a damage threshold function  $F_c(T, D)$  [6,12]:

$$dD = \frac{\frac{\partial C_{ijkl}(T, D)}{\partial D} \epsilon_{ij}^m d\epsilon_{kl}^m}{\frac{\partial F_c(T, D)}{\partial D}} \quad (6)$$

This damage evolution law can describe microcracking damage caused by tensile stresses and/or shear damage caused by shear stresses [4]. Both tensile and shear strains contribute to increase damage, however damage is not activated under a compressive state of stress since we assume here that microcracking does not occur under a compressive stress state. The thermal and swelling strains are related to the mechanical strain as:  $\epsilon_{ij}^m = \epsilon_{ij} - \epsilon_{ij}^{\text{th}} - \epsilon_{ij}^s$ , thus the thermal expansion and swelling effects directly govern the damage evolution law in Eq. (6). Damage evolution is computed incrementally according to Eq. (5) until attaining the saturation state at which  $D = D_{\text{cr}}$ , and the material fails and can no longer carry loads. Fracture is predicted to occur if  $D = D_{\text{cr}}$  and is captured by a vanishing element technique [13,14]. In this work, to quantify how close the material is to fracture, a failure indicator is defined by the ratio  $D/D_{\text{cr}}$ . Accordingly, fracture occurs when the failure indicator equals unity but the degree of damage is also tracked in this model.

### 3. Identification of model parameters

#### 3.1. Thermoelastic properties

A coherent and consistent set of material properties data needs to be established for the analysis. First, we refer to [7] for the thermoelastic properties for CVD-SiC as a function of temperature.

While published properties data can be found for the MAX phase  $\text{Ti}_3\text{SiC}_2$  [15–18], no data is available for the MAX phase  $\text{Ti}_3\text{SiC}_2/\text{SiC}$  composite joint that was processed when the THG specimens were made using the displacement reaction between SiC and TiC. In this paper, Mori-Tanaka models [19,20] using Eshelby's equivalent inclusion method [21] termed the Eshelby-Mori-Tanaka approach (EMTA) [22] are used to predict the thermoelastic properties (elastic modulus and CTEs) of the  $\text{Ti}_3\text{SiC}_2/\text{SiC}$  composite considering 0.5 volume fraction of  $\text{Ti}_3\text{SiC}_2$  uniformly distributed in the SiC matrix.

For the CVD-SiC, the functional representation by Snead et al. [7] is used to obtain the elastic modulus of SiC as a function of temperature:

$$E = E_0 - BT \exp\left(\frac{T}{T_0}\right) \quad (7)$$

where  $E_0 = 460$  GPa,  $B = 0.04$  GPa/K and  $T_0 = 962$  K. The evolution of  $E$  with temperature expressed in degrees centigrade is given in Fig. 2, which also presents the data from Barsoum et al. [15] for  $\text{Ti}_3\text{SiC}_2$  and predicted results by EMTA for the  $\text{Ti}_3\text{SiC}_2/\text{SiC}$  composite. Fig. 3 presents the CTE evolution with temperature predicted by EMTA for  $\text{Ti}_3\text{SiC}_2/\text{SiC}$ . On the same figure are also provided the measured values by Gao et al. [18] and Barsoum et al. [17] for  $\text{Ti}_3\text{SiC}_2$  and data from Ref. [7] for CVD-SiC.

#### 3.2. Stiffness reduction law

This section discusses the concepts of *continuum damage mechanics* (CDM) that our model employs. It then justifies the linear stiffness reduction law used in Eq. (2) for the brittle ceramics studied in this paper. In CDM originally due to Kachanov [23], damage is defined as the reduction in an elasticity property due to a reduction of the internal force-transmitting area that is caused by the occurrence and growth of microcracks and microvoids. Thus, in a damage process, the elastic modulus is reduced [10]. The *phenomenological* approach of CDM does not treat the individual microcracking mechanisms and their discrete evolutions, but it replaces the damaged material by an equivalent continuum and

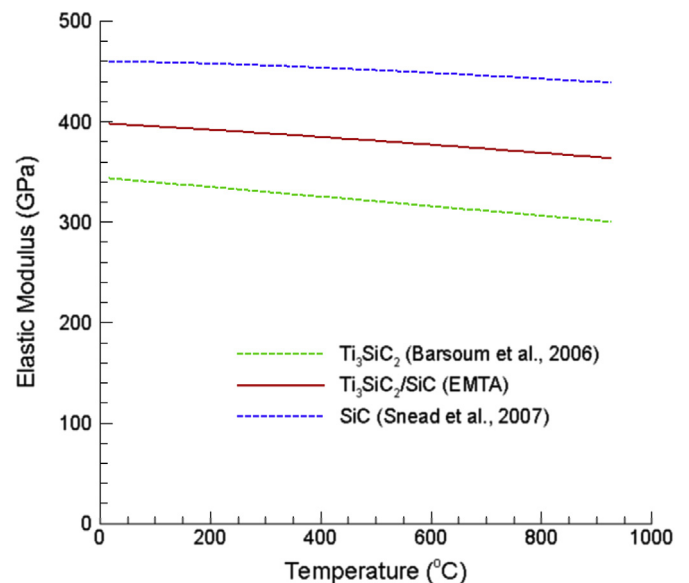


Fig. 2. Temperature-dependent elastic modulus for  $\text{Ti}_3\text{SiC}_2$  [15],  $\text{Ti}_3\text{SiC}_2/\text{SiC}$  composite (EMTA prediction), and CVD-SiC [7].

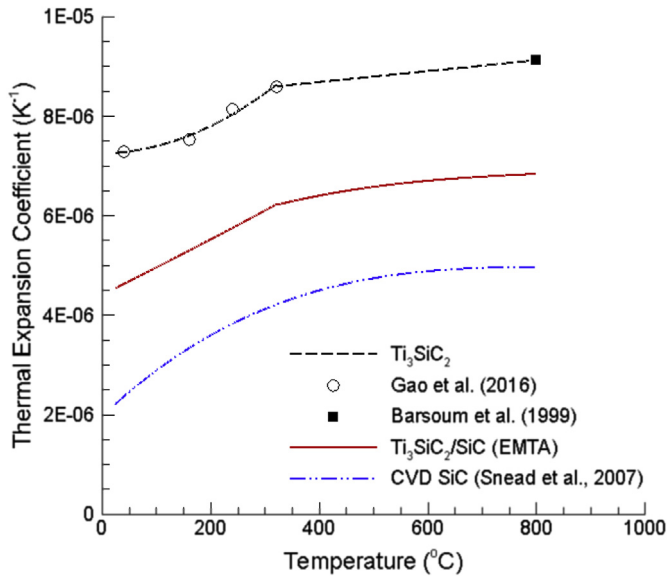


Fig. 3. Temperature-dependent CTE for  $\text{Ti}_3\text{SiC}_2$  [17,18],  $\text{Ti}_3\text{SiC}_2/\text{SiC}$  composite (EMTA prediction), and CVD-SiC [7].

homogeneous material with reduced elastic stiffness. The elastic stiffness evolution with loading is described by one or possibly several damage variables, which are the internal variables in the framework of thermodynamics of continuous media.

As microcracking is the key damage mechanism occurring in brittle ceramics, we use a single scalar damage variable ( $D$ ) to describe the damage process in these materials. Theoretically,  $D$  can vary from 0 to 1. However, a brittle ceramic element will break before  $D$  could reach 1. In this paper, the material fails and can no longer carry loads if  $D$  attains a critical value,  $D_{cr}$ . The next section will discuss the values of  $D_{cr}$  prescribed for CVD SiC and  $\text{Ti}_3\text{SiC}_2/\text{SiC}$ .

The simple linear stiffness reduction relation with the damage variable  $C_{ijkl} = C_{ijkl}^0(1 - D)$  (Eq. (2)) or in terms of elastic modulus  $E = E_0(1 - D)$  for isotropic damage was already used by different authors [6,9–11]. In this section, we demonstrate the soundness and accuracy of such a linear stiffness reduction law for CVD SiC. The demonstration is similar for the homogenized  $\text{Ti}_3\text{SiC}_2/\text{SiC}$  composite. We start from a virgin CVD SiC with the mean initial elastic modulus of 460 GPa according to [7]. We then consider this CVD SiC to contain a uniform distribution of spherical microvoids or completely random elongated microcracks, and look for determining its elastic stiffness as a function of the microvoid or microcrack volume fraction. To this end, the EMTA [19–22] was applied to the CVD SiC in both cases. In the EMTA, microvoids or microcracks were modeled as inclusions with zero stiffness, and in the latter case, the crack orientation averaging procedure proposed in Ref. [24] was also applied. The overall behavior of the damaged CVD SiC remains isotropic. Fig. 4(a) reports the results of the elastic modulus reduction as a function of the microvoid or microcrack volume fraction for both cases. Random elongated microcracks reduce the modulus to a larger extent than distributed microvoids do. We have found that the reduction of CVD SiC's elastic modulus versus void volume fraction agrees well with Rug et al.'s data [25] discussed in Ref. [7]. As  $D = 1 - E/E_0$ , the modulus results presented in Fig. 4(a) can be expressed in terms of the damage variable  $D$  and reported in Fig. 4(b) that proves the linear relationship of the modulus reduction with  $D$ . Fig. 4(b) clearly illustrates the basic concept of continuum damage mechanics that does not describe individual microcracks or voids, but the effect of voids or

microcracks on the elastic stiffness is captured phenomenologically through a damage variable.

### 3.3. Stress-strain behavior

The integration of the constitutive relation involving damage requires identification of the thermomechanical properties including the damage threshold function as a function of temperature for the temperature range of interest. The thermoelastic properties for all the materials of the THG joint specimen are discussed in the previous section. This section discusses the determination of the damage threshold function  $F_c(T, D)$  used in Eq. (6). For a given temperature, this function can be computed using the method described in Ref. [6] for the damage variable values in the  $[0, D_{cr}]$  interval using the thermodynamic force associated with the damage variable ( $F(T, D) = \partial\Phi(T, D)/\partial D$ ) and the stress-strain response at the same temperature.  $D_{cr}$  is the critical value of the damage variable at damage saturation.  $D_{cr}$  is small for brittle materials in tension, and this is the case for ceramic materials studied in this work.  $D_{cr} = 0.2$  is assumed for the SiC material of the THG specimen studied in this paper as previously used in Ref. [4].

The uniaxial tensile stress-strain responses for CVD-SiC as functions of temperature are estimated considering the stability of CVD-SiC mechanical properties in the  $[25^\circ\text{C}, 800^\circ\text{C}]$  temperature range of interest [7]. In addition, we assume the failure strain to be 0.1% at any temperature in this range, and this value of failure strain corresponds to the critical value of the damage variable,  $D_{cr} = 0.2$  [4]. Next, using the elastic modulus as a function of temperature presented in Fig. 2 and the linear stiffness reduction relation with the damage variable, the stress-strain response of CVD-SiC as a function of temperature is computed in this temperature range and illustrated in Fig. 5(a) for four selected temperatures. Our method to estimate the CVD-SiC stress-strain response leads to strength values varying from ~354 to 368 MPa, which correspond to the order of magnitude for the characteristic strength of bulk CVD-SiC reported in Ref. [7]. Finally, using the method described in Ref. [6], the damage threshold function for CVD-SiC is computed in the  $[25^\circ\text{C}, 800^\circ\text{C}]$  range and illustrated in Fig. 5(b) for four selected temperatures in this range.

While the mechanical behavior of CVD-SiC varies little with temperature the  $[25^\circ\text{C}, 800^\circ\text{C}]$  range, Henager and Kurtz [3] have observed that the bending strength and toughness of hot-pressed  $\text{Ti}_3\text{SiC}_2/\text{SiC}$  increased with temperature in this range. These findings can be used to estimate the tensile stress-strain response of the  $\text{Ti}_3\text{SiC}_2/\text{SiC}$  bulk as a function of temperature. However, the  $\text{Ti}_3\text{SiC}_2/\text{SiC}$  bonding layer is 15- $\mu\text{m}$  thick. Without or with negligible microdefects, the strength of this MAX phase composite at the micron scale must be significantly higher than the strength of the corresponding bulk material measured via bending tests of macroscopic specimens [3]. This problem is known as the size effect on the material strength that has been reported for various materials including metals and ceramics [7]. While fracture of the bulk ceramic is controlled by preexisting flaws or microvoids that quickly link up to form microcracks, a micron-scale ceramic that contains no flaws or only a few flaws should have much higher elongation at fracture (failure strain) than a bulk ceramic. From a continuum damage modeling standpoint, this is reflected by small values of the damage variable at fracture,  $D_{cr}$ . As for CVD-SiC, we consider the temperature-dependent elastic modulus of  $\text{Ti}_3\text{SiC}_2/\text{SiC}$  given in Fig. 2 and the linear stiffness reduction relation with the damage variable. The stress-strain response of the micron-scale  $\text{Ti}_3\text{SiC}_2/\text{SiC}$  is then computed as a function of temperature in the  $[25^\circ\text{C}, 800^\circ\text{C}]$  range assuming failure strain varying from 0.4% to 0.5% with  $D_{cr}$  from 0.13 to 0.15. The results for stress-strain response and damage threshold function for the micron-scale  $\text{Ti}_3\text{SiC}_2/\text{SiC}$  at



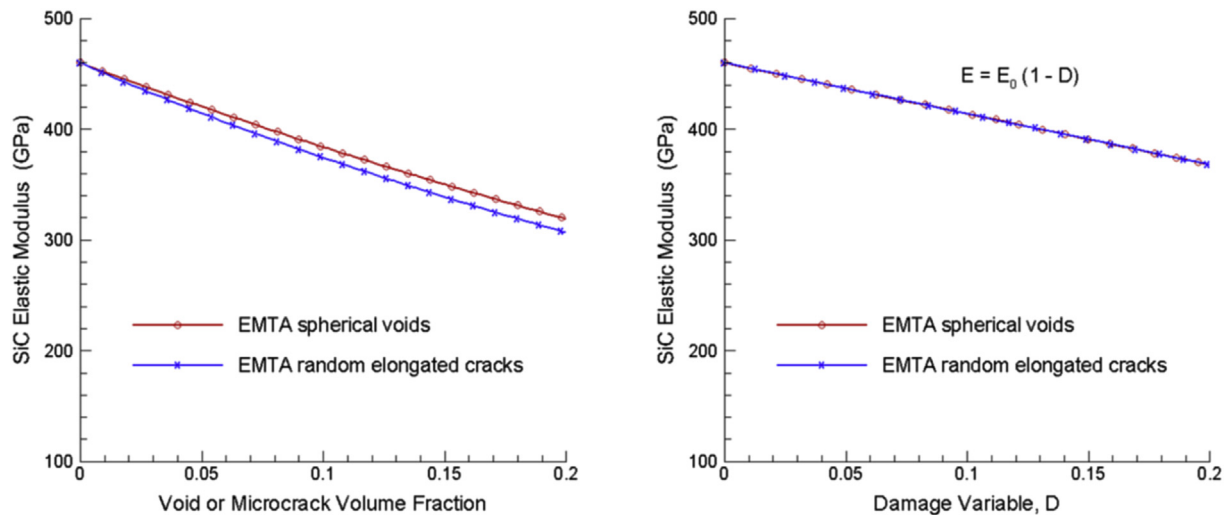


Fig. 4. (a) Elastic modulus reduction vs. void or microcrack volume fraction predicted by EMTA, and (b) results from (a) converted in terms of damage variable  $D$  limited to  $D = D_{cr}$ .

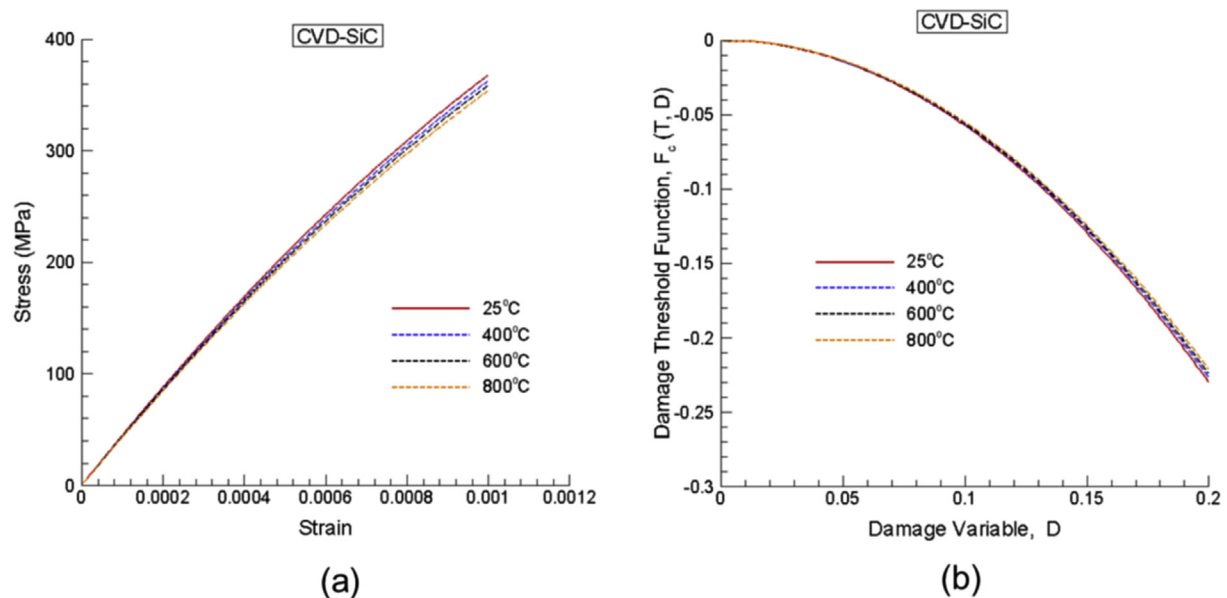


Fig. 5. (a) Assumed temperature-dependent uniaxial tensile stress-strain responses for CVD-SiC, and (b) the damage threshold functions calculated from (a).

selected temperatures are illustrated in Fig. 6(a) and (b), respectively.

### 3.4. Irradiation-induced swelling

Application of the damage model accounting for irradiation-induced swelling requires the knowledge of the saturation swelling strain,  $S_{max}$ , for a given material in the range of irradiation dose and temperature considered. Snead et al. [7] gathered and published swelling data from various studies for high-purity CVD-SiC. This work uses the data collected in Ref. [7] for the saturable point defect swelling regime of CVD-SiC (in the 25-to-1000 °C range). Accordingly,  $S_{max}$  values for SiC irradiated at 300 °C, 400 °C, 500 °C, and 800 °C are 2.1%, 2%, 1.4% and 0.8%, respectively.

Recently limited swelling data for the  $Ti_3SiC_2$  MAX phase has been published [26], but similar data for a  $Ti_3SiC_2$ /SiC composite are not available. Therefore, a method to predict swelling of this composite induced by neutron irradiation in the same ranges of

irradiation dose and temperature as for the constituent SiC and  $Ti_3SiC_2$  is needed. To this end, we develop in this paper a microstructural dual-phase model for  $Ti_3SiC_2$ /SiC in which each phase of the composite is discretized and allowed to reach the maximum swelling strain corresponding to the experimental swelling data [7,26] at a prescribed irradiation temperature. A digital image of the  $Ti_3SiC_2$ /SiC joint microstructure was used to create a FE mesh of this dual-phase system using the OOF2<sup>1</sup> public domain software. This allowed a detailed discretization of the microstructure and the ability for ABAQUS® to assign individual constitutive laws to each phase. The meshed microstructure with the constituent phase distribution is shown in Fig. 7(a). Fig. 7(b) presents a local snapshot showing the high-resolution mesh at the interfaces between the SiC (colored in blue) and the ternary MAX  $Ti_3SiC_2$  (yellow) phase.

In order to solely capture the irradiation-induced swelling of the

<sup>1</sup> Software developed at the National Institute of Standards and Technology.

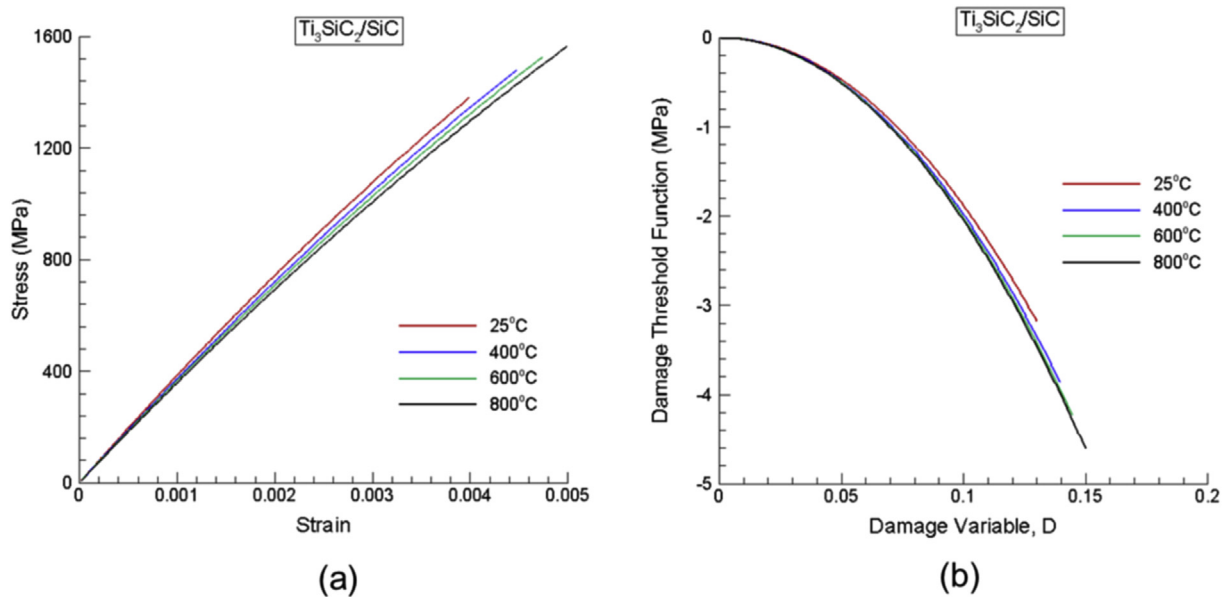


Fig. 6. (a) Assumed temperature-dependent uniaxial tensile stress-strain responses for  $\text{Ti}_3\text{SiC}_2/\text{SiC}$ , and (b) the damage threshold functions calculated from (a).

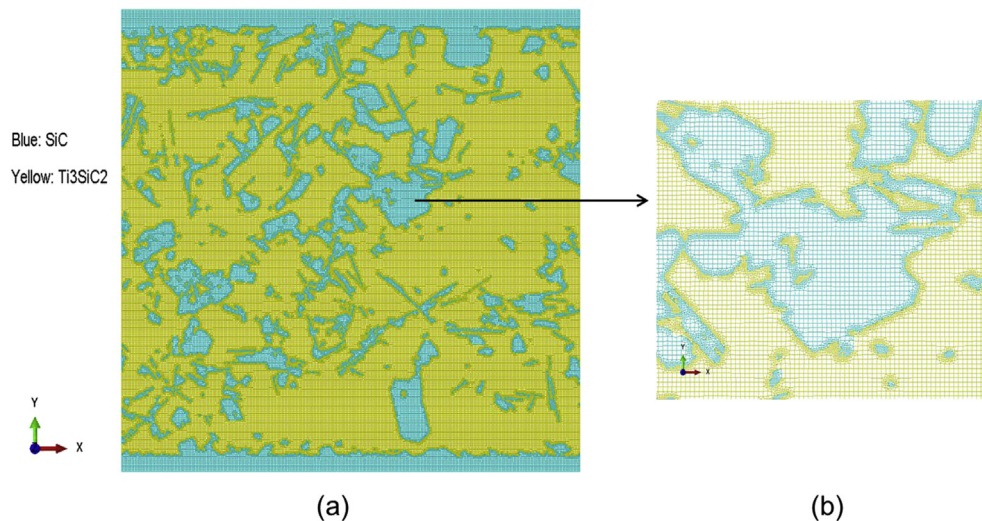


Fig. 7. (a) The dual-phase finite element mesh of the  $\text{Ti}_3\text{SiC}_2/\text{SiC}$  joint microstructure, and (b) a local snapshot showing the detailed mesh.

$\text{Ti}_3\text{SiC}_2/\text{SiC}$  composite without thermal expansion, the dual-phase microstructure model was assumed to be initially and uniformly at a prescribed irradiation temperature. Next, irradiation-induced swelling was applied to each constituent phase and allowed to evolve to the respective maximum value. Plane-stress conditions were assumed in the analysis. The boundary conditions applied to the microstructure model did not cause mechanical deformation but allowed the model to freely deform due to swelling at the prescribed irradiation temperature. Fig. 8(a–d) show the maximum levels attained in the constituent phases at the irradiation temperatures of 300 °C, 400 °C, 500 °C, and 800 °C, respectively. The SiC saturation swelling levels were taken from Ref. [7] and those for  $\text{Ti}_3\text{SiC}_2$  from Ref. [26]. The value at 300 °C for  $\text{Ti}_3\text{SiC}_2$  was obtained by a linear extrapolation from the measured value at 400 °C. Saturation swelling of SiC at 300 °C is the highest (2.1%) while at 800 °C maximum swelling considered for  $\text{Ti}_3\text{SiC}_2$  is the highest and is 1.47% according to [26].

As the dual-phase microstructure deformed solely due to

irradiation-induced swelling, the predicted overall volumetric strain attained at the maximum swelling level represents the maximum swelling,  $S_{\text{max}}$ , predicted for the  $\text{Ti}_3\text{SiC}_2/\text{SiC}$  composite. The dual-phase microstructural model was built from a digital image of the composite microstructure whose phase distributions and volume fractions vary locally. In the present model (Fig. 7(a)), the volume fractions of  $\text{Ti}_3\text{SiC}_2$  and SiC are about 0.7 and 0.3, respectively although the mean volume fraction of each phase is about ~0.5. Therefore, from the swelling values predicted for the  $\text{Ti}_3\text{SiC}_2/\text{SiC}$  composite with 0.7 volume fraction of  $\text{Ti}_3\text{SiC}_2$ , it is necessary to estimate the corresponding values for the  $\text{Ti}_3\text{SiC}_2/\text{SiC}$  composite with 0.5 volume fraction for each phase as illustrated in Fig. 9. This figure reports the swelling values predicted by the dual-phase model for the MAX phase 0.7-volume fraction composite that line up very well with the swelling levels from Ref. [7] for SiC and from Ref. [26] for  $\text{Ti}_3\text{SiC}_2$ . As a result, the swelling values of the 50%- $\text{Ti}_3\text{SiC}_2$ /50%-SiC composite were determined from these plots and have subsequently been used in the thermomechanical analysis of

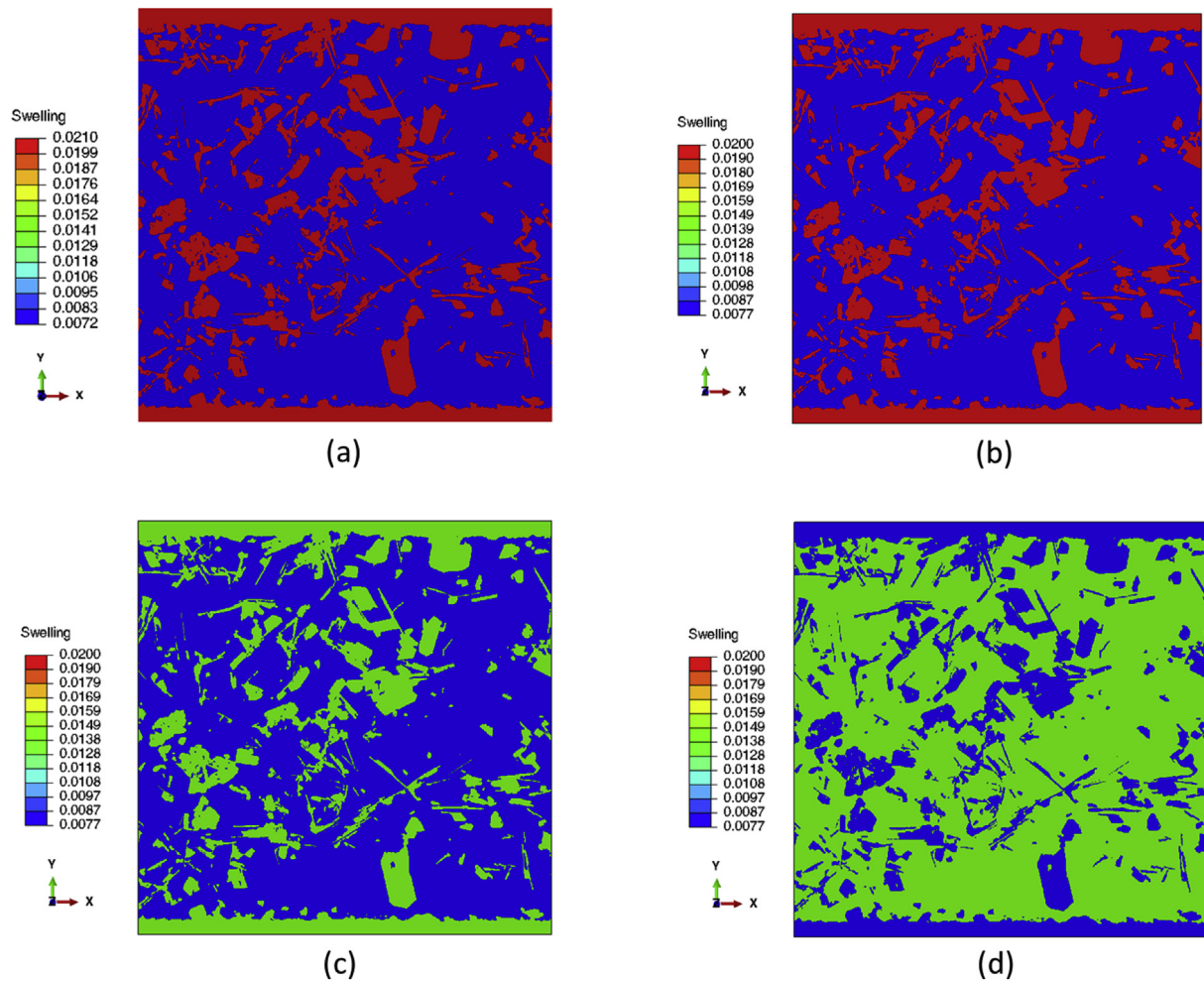


Fig. 8. Simulated irradiation-induced swelling at the maximum prescribed values at (a) 300 °C, (b) 400 °C, (c) 500 °C, and (d) 800 °C.

the THG joint specimen subjected to irradiation-induced swelling at the irradiation temperatures considered in this work.

#### 4. Results and discussion

The CDM model (Section 2.2) incorporating thermal expansion combined with irradiation-induced swelling effects was implemented in ABAQUS® by means of user-subroutines. It was then used with ABAQUS® to analyze the THG joint specimen subjected to heating followed by irradiation-induced swelling at a prescribed irradiation temperature, and cooling to room temperature after irradiation swelling. The analyses were performed for four cases corresponding to irradiation temperatures: 800 °C, 500 °C, 400 °C and 300 °C. The 800 °C case was first analyzed as the experimental observation of joint damage after neutron irradiation had been reported for this case [1]. The three-dimensional (3D) FE mesh of the THG joint specimen used in all the analyses and the associated material assignment are given in Fig. 10(a) and (b). The specimen is simply fixed at its bottom surface while its other surfaces are not constrained so that it can freely deform due to temperature change or irradiation-induced swelling.

##### 4.1. 800 °C case

In this case, the specimen is first uniformly heated from room temperature to 800 °C. Next, it is incrementally subjected to

irradiation-induced swelling at 800 °C to the swelling levels corresponding to the maximum values given in Fig. 9 (0.8% for SiC [7] and ~1.13% for  $\text{Ti}_3\text{SiC}_2/\text{SiC}$ ). Fig. 11(a) and (b) show the damage distributions at the ends of heating and of irradiation-induced swelling at this temperature. A view through a vertical section is shown in Fig. 11. Minor damage is accumulated at the notch as a result of heating, and further damage in this region including the joint and adjacent SiC is found under irradiation-induced swelling. Fig. 11(a) and (b) show that only minor and localized damage is predicted in the notch region. To understand the damage distribution, we examine the radial and hoop stresses in the specimen. Fig. 12(a) and 12(c) show the radial and hoop stress contours after heating to 800 °C. The  $\text{Ti}_3\text{SiC}_2/\text{SiC}$  joint with lower elastic modulus but higher thermal expansion coefficient than the SiC substrates (Figs. 2 and 3) is constrained to expand under heating resulting in compressive stresses for the joint but tensile stresses for SiC. Tensile stresses in the SiC substrates are not significant (Fig. 12(a–c)) except at the notch and in the vicinity of the joint (Fig. 12(b)) where relatively significant tensile radial stresses are observed and are responsible for minor damage in this region. The hoop stress distribution in the specimen shown in Fig. 12(c) is compressive in the joint and slightly tensile in the SiC substrate. The axial stresses  $\sigma_{aa}$  are negligible, such that the stress state in the joint is basically compressive and does not cause damage of the joint according to the damage model. Therefore, minor damage is predicted to occur in the notch area and along the immediate SiC/joint interface where



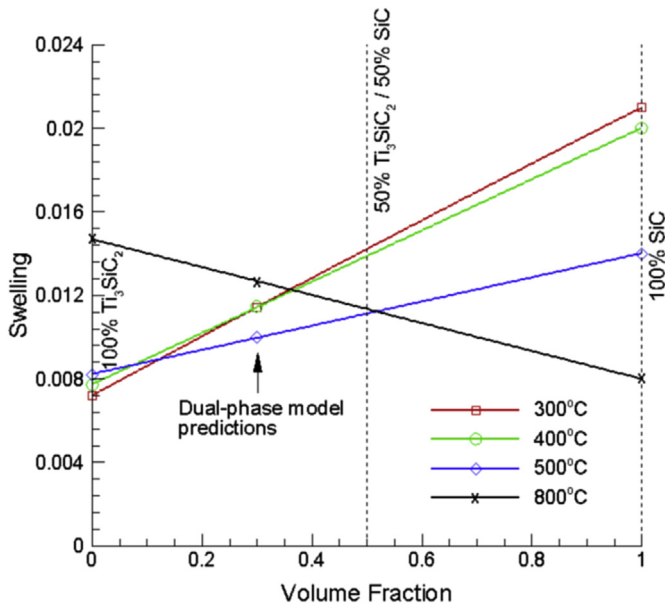


**Fig. 9.** Saturation swelling levels from Ref. [7] for SiC, experimental values from Ref. [26] for  $\text{Ti}_3\text{SiC}_2$  at 400 °C, 500 °C, and 800 °C. The value at 300 °C for  $\text{Ti}_3\text{SiC}_2$  was obtained by a linear extrapolation from the measured value at 400 °C. The swelling for the  $\text{Ti}_3\text{SiC}_2/\text{SiC}$  composite with 50% volume fraction of each constituent is obtained from these plots for each irradiation temperature.

tensile radial stresses develop. Damage slightly affects the joint in this area but is mainly interfacial.

Subject to irradiation-induced swelling at 800 °C up to the respective maximum levels, further damage is observed at the notch area but damage remains low as the failure indicator is much less than unity (Fig. 11(b)). Further damage during swelling is caused by more pronounced concentrations of tensile radial stresses in this area as the higher swelling joint material is constrained in its expansion by the lower swelling SiC. After irradiation swelling, the THG specimen is uniformly cooled to room temperature. The damage development at the end of cooling presented in Fig. 13(a) and (b) clearly shows localized damage in the notch area and its vicinity. During cooling the thermal stresses and strains vanish, but swelling strains remain. The mismatch of swelling strains between the joint and the SiC substrate (Fig. 9) has caused more damage for the joint and SiC in the notch area, but damage remains limited to this area. Fig. 13(a) and (b) also indicate that the

joint has not failed after cooling to room temperature following irradiation-induced swelling at 800 °C. Damage prediction for the 800 °C case is consistent with the SEM observation by Katoh et al. [1] for this case. These authors observed microcracks in the bonding layer after the irradiation experiment, but the interface bonding appeared to be intact before the forced debond (by a torsion test). It is also noteworthy that in this case, the THG specimen only suffered minor damage at the notch as predicted (Fig. 13) and the joint's shear strength was only slightly reduced compared to the value for the unirradiated specimen as found in subsequent torsion testing [1]. Significantly, however, the fracture mode changed from bulk failure that fully involves the SiC substrate and the entire THG for the unirradiated case to a more planar fracture that is localized to a much greater extent in the plane of the joint region. This is indicative of changes to the THG joint/SiC interface as predicted by the CDM.

#### 4.2. 500 °C case

The specimen is uniformly heated to 500 °C. It is then subjected to incremental swelling caused by neutron irradiation until reaching the respective maximum swelling levels at 500 °C (1.4% for SiC [7] and ~1.11% for  $\text{Ti}_3\text{SiC}_2/\text{SiC}$ , Fig. 9). Fig. 14(a) and (b) show the damage distributions at the end of irradiation-induced swelling at 500 °C, and after cooling to room temperature. Compared to the 800 °C case, heating to 500 °C and irradiation induced swelling at this temperature has caused significantly less damage at the notch area in the SiC substrates adjacent to the joint due to the smaller mismatch of thermoelastic properties and differential swelling between the joint and SiC substrates. Examining Figs. 2 and 9 together reveal that the differential swelling acts to compensate for the differential thermal expansion to some extent during irradiation at a given temperature. This is because the CTE of the  $\text{Ti}_3\text{SiC}_2/\text{SiC}$  composite (Fig. 2) is much higher than the CTE for SiC at given temperature in the range of interest while the swelling of this MAX phase composite is lower than the value for SiC at the same irradiation temperature (except at 800 °C). The combined thermal expansion/differential swelling effect only induces minor damage to the joint at the maximum prescribed irradiation-induced swelling at 500 °C as shown in Fig. 14(a). However, cooling to room temperature after radiation-induced swelling at 500 °C has led to more significant damage development inside the whole layer of the joint as shown in Fig. 14(b). Thermal strains almost vanished during cooling to room temperature while the swelling strains persisted and have caused more significant damage to the joint.

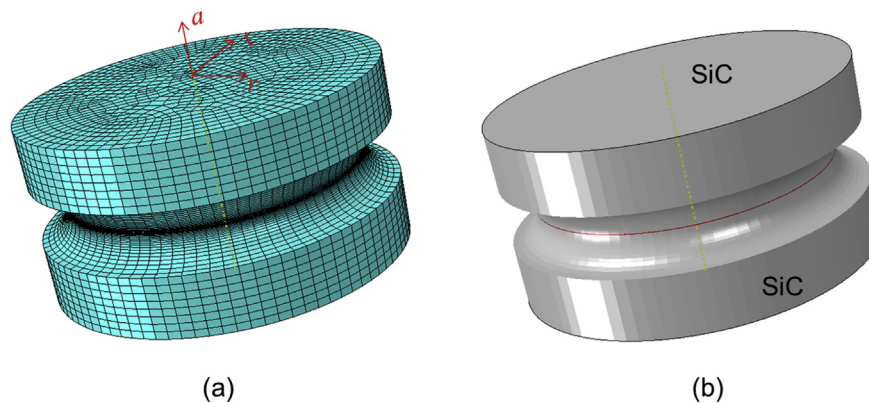


**Fig. 10.** (a) 3D finite element mesh of the THG joint specimen with a local cylindrical coordinate system,  $rta$  defined for stress/strain computations, and (b) material assignment showing the SiC substrates (colored in gray) joined by a 15- $\mu\text{m}$  thick  $\text{Ti}_3\text{SiC}_2/\text{SiC}$  layer (in red). (For interpretation of the references to colour in this figure legend, the reader is referred to the web version of this article.)



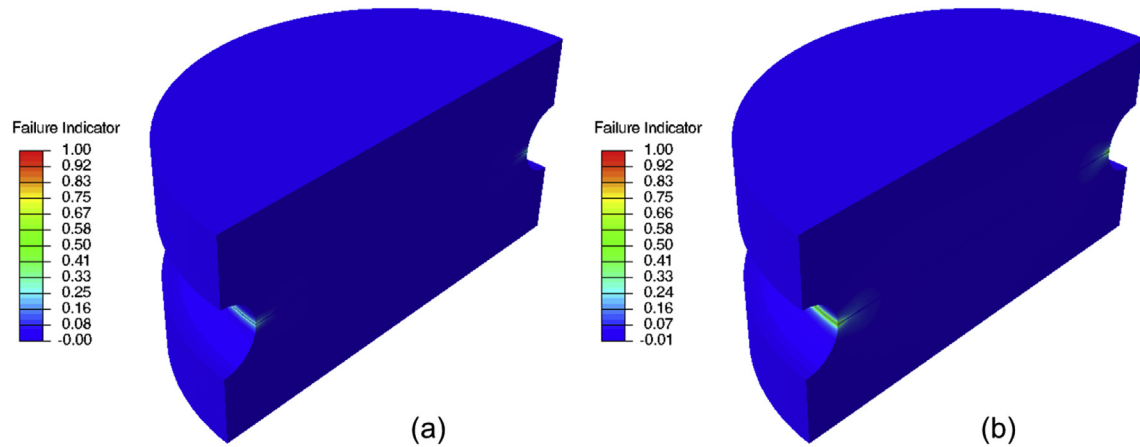


**Fig. 11.** (a) Damage distribution at the end of heating to 800 °C (view through a vertical section), and (b) further damage development due to irradiation-induced swelling at 800 °C.

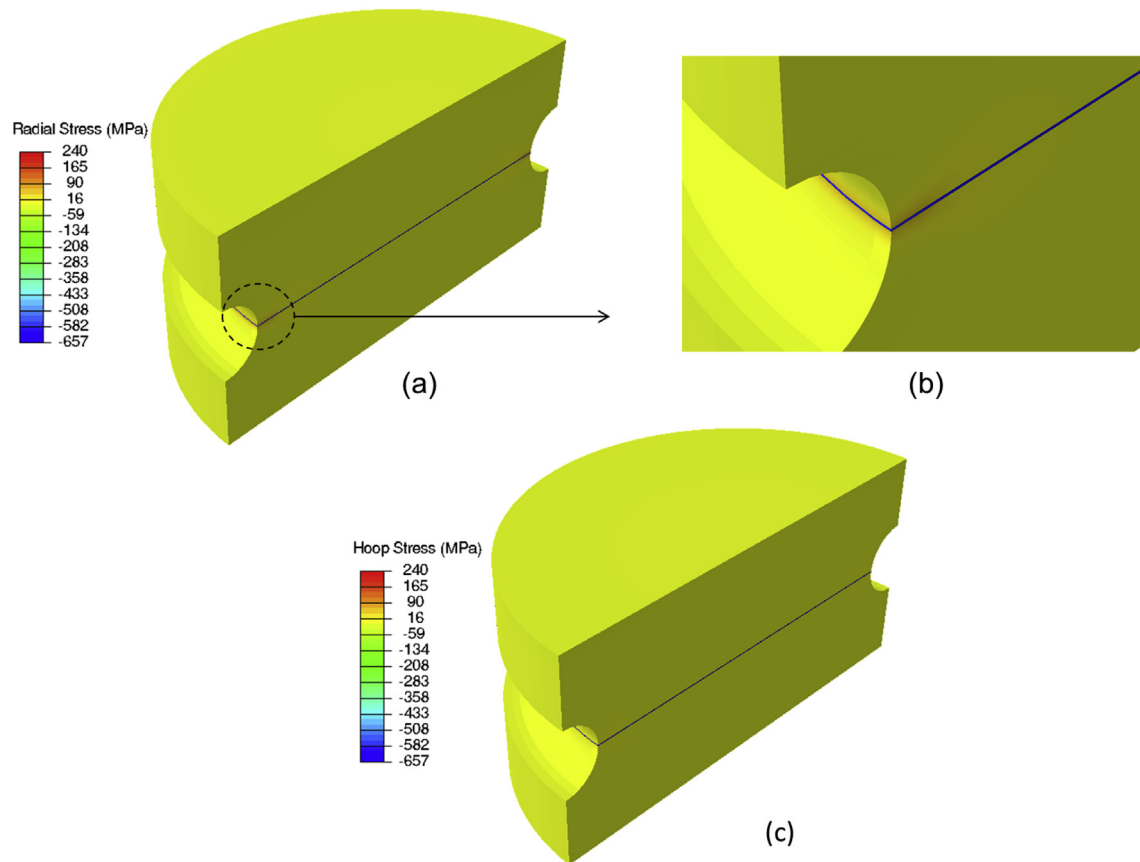


**Fig. 12.** (a) Radial stress distribution at the end of heating to 800 °C, (b) a zoom-in showing significant tensile radial stresses in the SiC substrates at the notch and adjacent to joint layer, and (c) hoop stress distribution at the end of heating to 800 °C.

Nevertheless, the joint is predicted to survive after cooling to room temperature as indicated by the failure indicator of about  $\sim 0.3$  (Fig. 14(b)). This finding agrees with recent experimental evidence of a  $\text{Ti}_3\text{SiC}_2/\text{SiC}$  joint irradiated at 530 °C to 20 dpa showing minimal damage.<sup>2</sup>

With regard to lower temperature irradiations and the lack of

time-dependent deformation mechanisms in the current model, Katoh et al. [27] observed a possible mechanism of irradiation creep that might mitigate swelling-induced stress buildup, thus reducing damage accumulation. However, to the best of our knowledge, no irradiation creep data on  $\text{Ti}_3\text{SiC}_2$  and  $\text{Ti}_3\text{SiC}_2/\text{SiC}$  are available that could be used to perform an analysis including this mechanism. The predicted damage distribution is thus due to the swelling mismatch between the joint and SiC substrates causing tensile stresses in the joint. Although damage has expanded in the joint, it has not attained the critical level needed to fail the joint by thermal

<sup>2</sup> Y. Katoh and T. Koyanagi, Oak Ridge National Laboratory, personal communication.

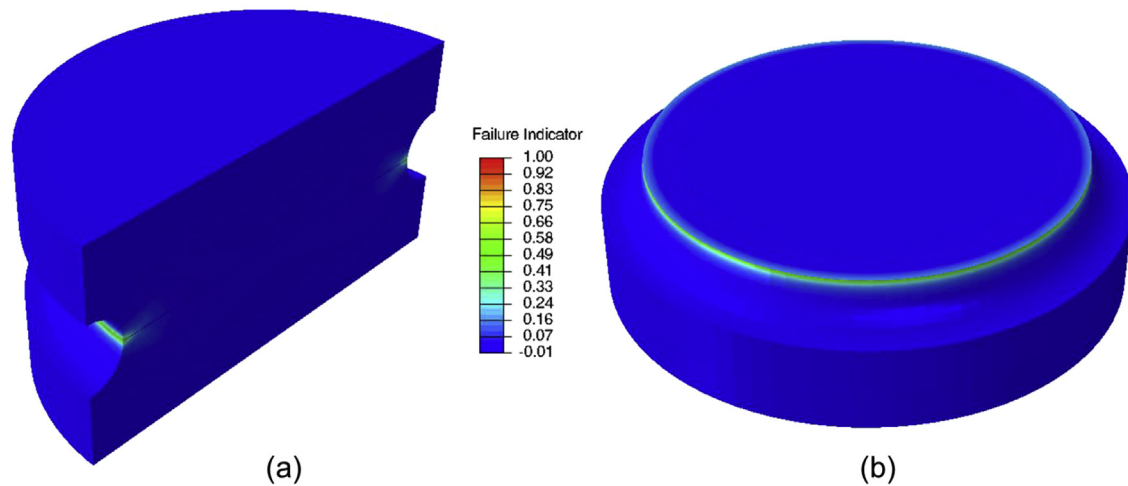


**Fig. 13.** Damage distribution after irradiation-induced swelling at 800 °C and cooling to room temperature (a) view through a vertical section, and (b) view through a horizontal section passing through the middle of the joint layer.

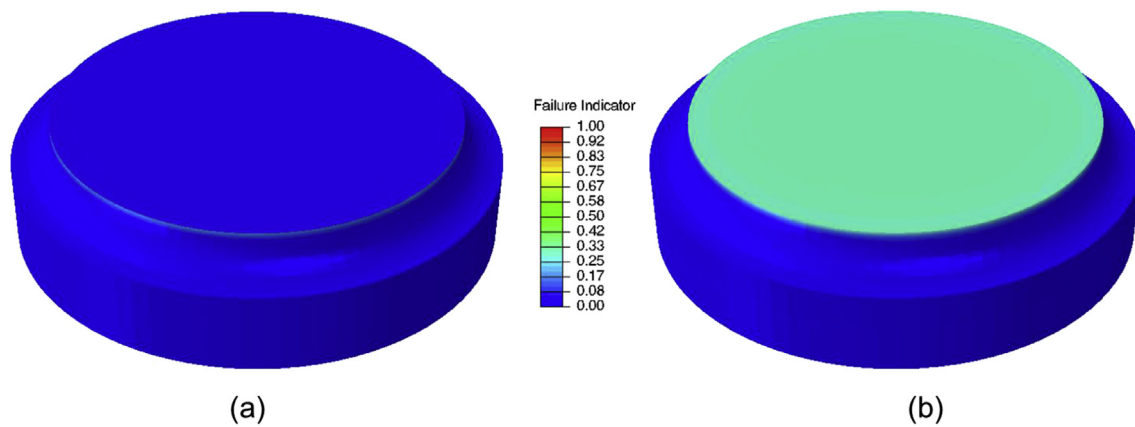


**Fig. 14.** Damage distributions (a) right after irradiation-induced swelling at 500 °C, and (b) after cooling to room temperature.

expansion/contraction combined with irradiation-induced swelling.

#### 4.3. 400 °C case

In this case, the THG specimen is uniformly heated to 400 °C. It is then subjected to incremental swelling caused by neutron irradiation until reaching the respective maximum swelling levels at 400 °C (2% for SiC [7] and 1.39% for  $\text{Ti}_3\text{SiC}_2/\text{SiC}$ , Fig. 9). First, very minor damage occurred at the notch due to the mismatched thermoelastic properties as explained for the previous cases. Nevertheless, during irradiation the important mismatch of irradiation swelling between these materials at 400 °C (Fig. 9) has caused significant tensile stresses in the joint inducing more significant damage to joint compared to the 500 °C case. Fig. 15(a) and (b) show the damage distributions at the end of irradiation-induced swelling at 400 °C, and after cooling to room temperature. Comparing Fig. 15(a) to Fig. 14(a), and Fig. 15(b) to Fig. 14(b) shows that irradiation at 400 °C has caused more substantial damage to the joint than irradiation at 500 °C. Fig. 9 shows that the differential swelling at 400 °C is about twice the level at 500 °C, this explains why more significant damage is predicted for the joint irradiated at 400 °C. Higher differential swelling also has caused more damage after the joint was cooled to room temperature.

#### 4.4. 300 °C case

The 300 °C case is similar to the 400 °C case, it is also studied here due to a recent irradiation experiment reported in Ref. [5] on  $\text{Ti}_3\text{SiC}_2/\text{SiC}$ -joined CVD SiC at ~300 °C. As we mentioned earlier, in Ref. [5], the 150- $\mu\text{m}$  joint was formed from the reaction sintering with a Ti-Si-C system according to proprietary process methods, which were different from the 15- $\mu\text{m}$  joint formed by a tape casting process to join ceramics using a displacement reaction between SiC and TiC [2,3]. Amid these differences, it is still meaningful to qualitatively compare the damage prediction for this case to experimental observations to assess the model.

In the 300 °C case, the differential swelling between the  $\text{Ti}_3\text{SiC}_2/\text{SiC}$  joint and SiC substrates is the largest compared to the values for all the previous cases (Fig. 9). After heating the THG specimen uniformly to 300 °C, incremental swelling caused by neutron irradiation was applied until reaching the respective maximum swelling levels at 300 °C in the specimen (2.1% for SiC [7] and 1.41% for  $\text{Ti}_3\text{SiC}_2/\text{SiC}$ , Fig. 9). Fig. 16(a) and (b) show the damage distributions at the end of irradiation-induced swelling at 300 °C, and after cooling to room temperature. Compared to the 400 °C case, higher differential swelling has caused more damage to the joint (Fig. 16(a)), and damage has reached an advanced state (the failure indicator exceeding 0.7) after cooling the specimen to room temperature (Fig. 16(b)). The damage distribution presented in

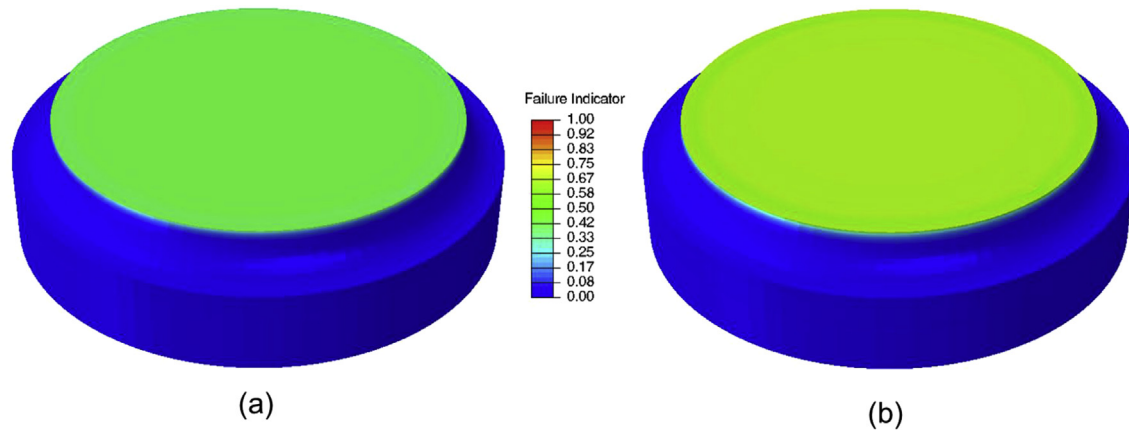


Fig. 15. Damage distributions (a) right after irradiation-induced swelling at 400 °C, and (b) after cooling to room temperature.

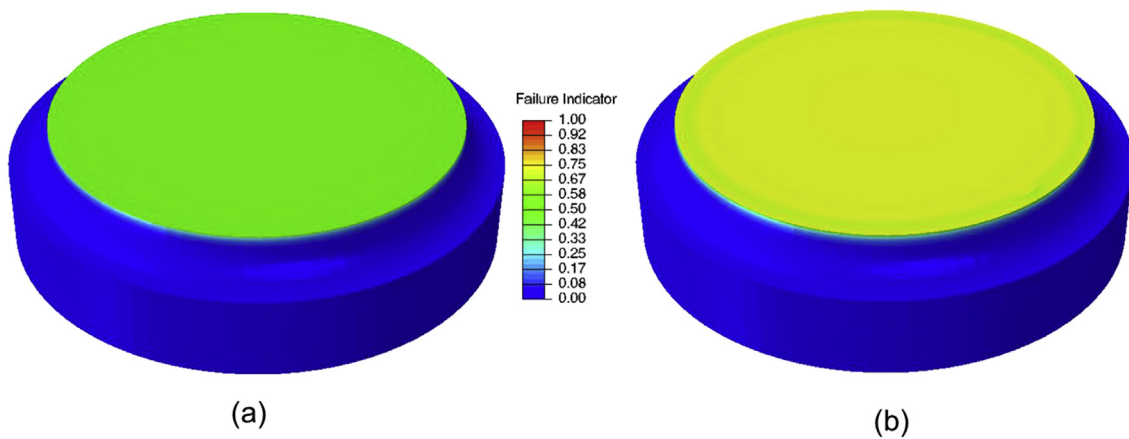


Fig. 16. Damage distributions (a) right after irradiation-induced swelling at 300 °C, and (b) after cooling to room temperature.

Fig. 16(b) indicates that the joint has suffered significant microcracking although the joint still survived. The irradiation experiment performed in Ref. [5] for this type of joint revealed many microcracks within the irradiated joint, and microcracking was attributed to the irradiation. The experimental observations in Ref. [5] have then qualitatively confirmed by the model prediction for the 300 °C case. Table 1 summarizes our findings regarding damage development in the THG specimen from all the analyses using the damage model.

## 5. Conclusions

This paper develops a continuum damage mechanics model that incorporates thermal expansion combined with irradiation-

induced swelling effects to study the origin of cracking observed in some THG specimens subjected to heating to a prescribed temperature following by neutron irradiation at that temperature, and cooling to room temperature after irradiation. Micromechanical modeling using an Eshelby-Mori-Tanaka approach was applied to compute the thermoelastic properties of the  $\text{Ti}_3\text{SiC}_2/\text{SiC}$  composite joint needed for the damage model. In addition, a microstructural dual-phase  $\text{Ti}_3\text{SiC}_2/\text{SiC}$  model was also developed to estimate irradiation-induced swelling of the composite joint at a given temperature resulting from swelling of both SiC and the  $\text{Ti}_3\text{SiC}_2$  MAX phase. Four cases have been analyzed corresponding to three irradiation temperatures: 800 °C, 500 °C, 400 °C, and 300 °C. The following conclusions can be drawn from the analysis results:

**Table 1**  
Findings from damage analyses of the THG specimen.

Irradiation Temperature	SiC Substrates	$\text{Ti}_3\text{SiC}_2/\text{SiC}$ Joint
300 °C	Negligible damage	Negligible damage during heating – severe damage after irradiation swelling and cooling to room temperature
400 °C	Negligible damage	Negligible damage during heating –important damage after irradiation swelling and cooling to room temperature
500 °C	Negligible damage	Negligible damage during heating and irradiation swelling - moderate damage after cooling to room temperature
800 °C	Slightly damaged at the notch area	Slightly damaged at the notch area

- **800 °C case:** Minor localized damage is predicted at the notch and mainly affects the SiC substrates immediately adjacent to the bonding layer. Under combined thermal and irradiation-induced swelling the joint did not fail. The damage prediction for this case agrees with the available experimental observations.
- **500 °C case:** Subject to heating to 500 °C and irradiation swelling at this temperature, minor localized damage of the specimen is predicted at the notch. The joint underwent moderate damage after cooling to room temperature but did not fail.
- **400 °C case:** As in the previous cases, heating has only caused very minor damage at the specimen notch. However, the significant mismatch of irradiation-induced swelling at 400 °C has caused significant tensile stresses in the joint leading to important damage after irradiation and cooling to room temperature although the joint did survive.
- **300 °C case:** This is the most critical case because it represents the largest differential swelling between the MAX phase and SiC. Although heating only caused negligible damage, significant differential swelling caused severe damage to the joint after irradiation and cooling to room temperature. Although the joint survived, severe damage was predicted after cooling to room temperature. The damage prediction for this case agrees with the available experimental observations for a similar type of joint.

Although the results need additional experimental confirmations, the predictive modeling tool developed in this paper has been demonstrated to be effective and robust. The limited experimental observations appear to validate the modeling results in that only minor damage occurs in the joint for the 800 °C case, and at 530 °C (close to the 500 °C case), and with severe joint damage observed for the 300 °C case. Currently, the model lacks any time-dependent deformation mechanisms, such as irradiation creep, that could mitigate some of the predicted damage via stress relaxation. Such data exists for SiC but not for  $\text{Ti}_3\text{SiC}_2$  and, therefore, was not attempted here. Future work will include further model development incorporating the potentially stress relieving effects of irradiation-induced creep. An interesting aspect of the model results is that once a joint has reached saturation swelling at some temperature in the range considered the most damaging operation on an irradiated joint is cooldown from the irradiation temperature. It seems that this prediction has serious implications for thermal cycling of irradiated joints, which is particularly relevant for plasma devices operated in a pulsed mode where frequent thermal cycling is normal.

The developed tool should be able to support the neutron-irradiation based design of joined ceramics and composites in conjunction with in-reactor testing. The use of dual-phase or multi-phase materials for joining is a natural consequence of trying to

balance material properties and ease of joint fabrication via reaction synthesis methods. However, differential material responses, including thermal expansion and swelling, often result in damaging misfitting stresses that are not present in single-phase joints.

## Acknowledgements

This research was supported by U.S. Department of Energy (DOE), Office of Fusion Energy Sciences under Contract DE-AC05-76RL01830. PNNL is a multi-program national laboratory operated by Battelle Memorial Institute for the US DOE under DE-AC06-76RLO 1830.

## References

- [1] Y. Katoh, L.L. Snead, T. Cheng, C. Shih, W.D. Lewis, T. Koyanagi, T. Hinoki, C.H. Henager Jr., M. Ferraris, J. Nucl. Mater. 448 (1–3) (2014) 497–511.
- [2] R. Radhakrishnan, C.H. Henager, J.L. Brimhall, S.B. Bhaduri, Scr. Mater. 34 (1996) 1809–1814.
- [3] Henager Jr., R.J. Kurtz, J. Nucl. Mater. 417 (2011) 375–378.
- [4] C.H. Henager Jr., B.N. Nguyen, R.J. Kurtz, T.J. Roosendaal, B.A. Borlaug, M. Ferraris, A. Ventrella, Y. Katoh, J. Nucl. Mater. 466 (2015) 253–268.
- [5] T. Koyanagi, Y. Katoh, J.O. Kiggans, T. Hinoki, H.E. Khalifa, C.P. Deck, C.A. Back, J. Nucl. Mater. 488 (2017) 150–159.
- [6] B.N. Nguyen, B.J. Koeppel, S. Ahzi, M.A. Khaleel, P. Singh, J. Am. Ceram. Soc. 89 (4) (2006) 1358–1368.
- [7] L.L. Snead, T. Nozawa, Y. Katoh, T.-S. Byun, S. Kondo, D.A. Petti, J. Nucl. Mater. 371 (1–3) (2007) 329–377.
- [8] M. Ben-Belgacem, V. Richet, K.A. Terrani, Y. Katoh b, L.L. Snead, J. Nucl. Mater. 447 (2014) 125–142.
- [9] J. Lemaitre, J.-L. Chaboche, Mécanique des Matériaux Solides, Dunod, Paris, France, 1985.
- [10] G.A. Maugin, The Thermomechanics of Plasticity and Fracture, Cambridge University Press, Cambridge, UK, 1992.
- [11] J. Lemaitre, in: O. Allix, F. Hild (Eds.), Continuum Damage Mechanics of Materials and Structures, Elsevier Science Ltd, Oxford, UK, 2002, pp. 235–258.
- [12] J. Renard, J.P. Favre, T. Jeggy, Compos. Sci. Technol. 46 (1) (1993) 29–37.
- [13] V. Tvergaard, Int. J. Fract. 31 (3) (1986) 183–209.
- [14] B.N. Nguyen, V. Kunc, Int. J. Damage Mech. 19 (6) (2010) 691–725.
- [15] M.W. Barsoum, M. Radovic, A. Ganguly, T. Zhen, P. Finkel, S.R. Kalidindi, E. Lara-Curzio, Acta Mater. 54 (10) (2006) 2757–2767.
- [16] B. Manoun, S.K. Saxena, H.P. Liermann, M.W. Barsoum, J. Am. Ceram. Soc. 88 (12) (2005) 3489–3491.
- [17] M.W. Barsoum, T. El-Raghy, C.J. Rawn, W.D. Porter, H. Wang, E.A. Payzant, C.R. Hubbard, J. Phys. Chem. Solids 60 (4) (1999) 429–439.
- [18] H.R. Gao, W. Benitez, R. Son, M. Arroyave, Radovic, Mater. Sci. Engn A 676 (2016) 197–208.
- [19] T. Mori, K. Tanaka, Acta Metall. 21 (1973) 571–574.
- [20] Y. Benveniste, Mech. Mater. 6 (1987) 147–157.
- [21] J.D. Eshelby, Proc. R. Soc. Lond. 252 (1959) 561–569. Series A (Mathematical and Physical Sciences).
- [22] B.N. Nguyen, EMTA User's Guide, Pacific Northwest National Laboratory, Richland, WA, 2010.
- [23] L.M. Kachanov, Izv. Akad. Nauk. SSSR 8 (1958) 26.
- [24] S. Advani, C.L. Tucker, J. Rheol. 31 (1987) 751–784.
- [25] R. Ruh, A. Zagvil, J. Barlowe, Am. Ceram. Soc. Bull. 64 (1985) 1368.
- [26] C. Ang, S. Zinkle, C. Shih, C. Silva, N. Cetiner, Y. Katoh, J. Nucl. Mater. 483 (2017) 44–53.
- [27] K. Yutai, L.L. Snead, C.M. Parish, T. Hinoki, J. Nucl. Mater. 434 (2013) 141–151.